On the influence of dislocation walls in CdTe:Cl

Giulia Venturi, Antonio Castaldini, Eric Gros D'aillon, Camille Buis, Loick Verger, Anna Cavallini

Nuclear Instruments and Methods in Physics Research A 813 (2016) 68–73

Contents lists available at ScienceDirect

Nuclear Instruments and Methods in Physics Research A

journal homepage: www.elsevier.com/locate/nima

On the influence of dislocation walls in CdTe:Cl

Giulia Venturi [a,*], Antonio Castaldini [a], Eric Gros d'Aillon [b], Camille Buis [b], Loick Verger [b], Anna Cavallini [a]

[a] University of Bologna Alma Mater Studiorum, Department of Physics and Astronomy, Viale Berti Pichat 6/2, 40127 Bologna, Italy
[b] CEA, LETI, MINATEC-Campus, 17 Rue des Martyrs, F-38054 Grenoble, France

ARTICLE INFO

Article history:
Received 20 April 2015
Received in revised form
6 January 2016
Accepted 11 January 2016
Available online 16 January 2016

Keywords:
CdTe:Cl
Dislocation walls
Electronic levels
PICTS

ABSTRACT

Studies were performed on two types of chlorine-compensated cadmium telluride crystals with a different density of native dislocations walls. The crystals were investigated by current–voltage measurements, photo-induced current transient spectroscopy and absorption measurements, in the view of investigating the influence of the density of dislocation walls on their charge transport properties and electronic levels scheme. It results that a higher density of dislocation walls increases the dark current in CdTe. To the contrary, the optical absorption properties do not seem to be influenced by the presence of dislocation walls. The PICTS measurements demonstrated that a lower density of dislocation walls provides a higher concentration of compensation-related defects and a lower concentration of the defects responsible for the peaks observed at high temperature, possibly associated to donor-pair complexes.

1. Introduction

Cadmium telluride is a well-known II–VI compound, widely used in several applications such as infrared optical windows and lenses [1,2], thin film solar cells [3,4] and room-temperature radiation detectors for X-rays, gamma rays, beta particles and alpha particles [5].

CdTe is particularly suitable for the detection of high-energy photons because of its wide bandgap, which provides high resistivity and low leakage current. The high atomic number and high density of the elements also provide high X-ray stopping power [6].

In order to obtain high resistivity material ($\rho > 10^8\ \Omega$ cm), required for good detection performance, CdTe crystals are grown in Te-rich conditions. In this way, V_{Cd} acceptors produced during the growth can be compensated by group III or group VII donors, such as chlorine, thus obtaining the semi-insulating chlorine-compensated CdTe (CdTe:Cl) compound [7].

Although CdTe:Cl is characterized by an elevated charge carrier transport [8], the efficiency of CdTe-based detectors is nowadays limited by the presence of dislocations and other defects, which were reported to be responsible for the presence of lines in the images obtained with CdTe based X-ray detectors[9] and charge transport non-uniformities [10]. On the other hand, it should be pointed out that such defects were also described to act as intra-gap trapping centers for the charge carriers, rather than recombination centers, reducing the carrier recombination [11].

Given this, the characterization of the deep-levels associated to the dislocation walls promises to be a study of great interest.

In this work, we report about studies performed on two types of chlorine-compensated cadmium telluride crystals grown by Acrorad (Japan) by Travelling Heater Method (THM), with 7×8 mm^2 area and 480 μm thickness. The samples are all standard Acrorad products. The two types of crystals have an evidently different density of native dislocations walls, as shown in Fig. 1. Dislocation walls correspond to the arrangement of dislocations parallel to each other, in the same plane of the crystal. This arrangement creates a region where the crystal lattice is heavily distorted. The difference of orientation of each side of the wall is small, thus the dislocation walls are low angle subgrain boundaries[12].

The distribution of dislocations was investigated by etching the polished sample surface with Everson solution (6 mL HF, 24 mL HNO_3, 150 mL lactic acid). The samples were investigated with an Olympus BX61 microscope in reflection mode as described in [9]. A typical micrograph of the first type of samples is shown in Fig. 1(a). This kind of samples will be named from now on "samples with dislocation walls". A typical micrograph of the second type of samples is shown in Fig. 1(b). This kind of samples will be named from now on "samples without dislocation walls", for the sake of simplicity. Four samples were studied for each kind of crystal.

The two types of crystals were investigated by current–voltage (I–V) measurements, photo-induced current transient spectroscopy (PICTS) and absorption measurements.

* Corresponding author. Tel.: +39 051 2090108.
E-mail address: giulia.venturi4@studio.unibo.it (G. Venturi).

http://dx.doi.org/10.1016/j.nima.2016.01.031
0168-9002/

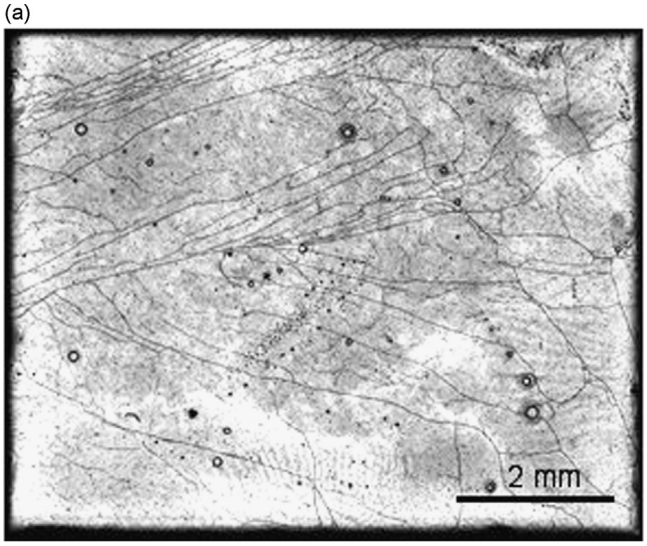

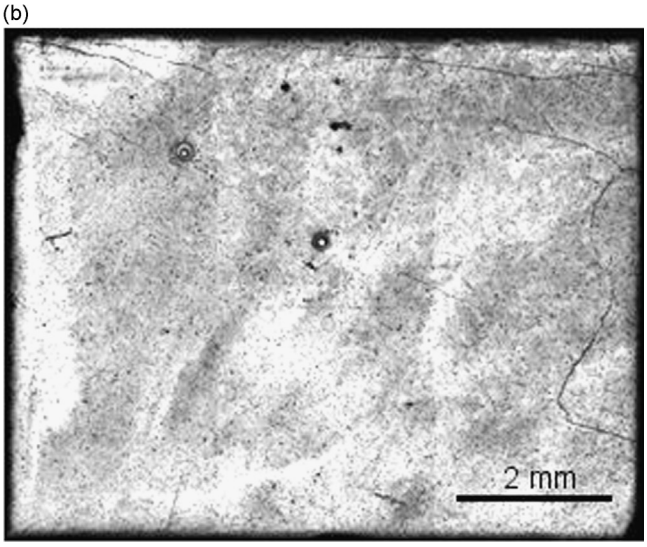

Fig. 1. Micrographs of the Te-face of the two types of CdTe:Cl crystals studied, taken with an Olympus BX61 microscope in reflection mode: (a) with dislocation walls and (b) without dislocation walls.

The aim of this study is to compare the charge transport properties and the electronic levels scheme of the two types of crystals in order to investigate how they can be influenced by dislocation walls.

2. Experiment and discussion

2.1. Current–voltage characteristics

In order to perform the *I–V* measurements two ohmic contacts were provided on the samples, in sandwich configuration (see sketch in Fig. 2). These contacts were obtained by a GaAl alloy, fabricated by immersing an aluminum sharp cylindrical stick (4 mm diameter) in a block of Ga at room temperature and subsequently painting the surface of the crystal with the stick, using a micromanipulator. The resulting contacts covered an area of 1.5×5 mm^2 (each) and showed ohmic characteristics (Fig. 2). The GaAl paste was used to easily manufacture ohmic electrical contacts with different geometries for the various tests. The two types of crystals, with and without dislocation walls, were primarily studied by comparing their current–voltage characteristics (Fig. 2),

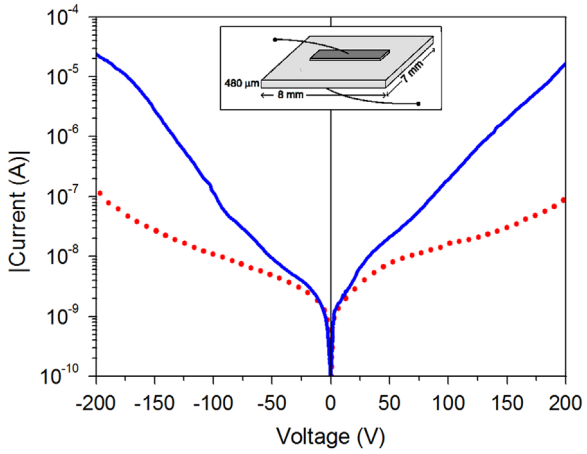

Fig. 2. Typical current–voltage characteristics of the samples with dislocation walls (solid blue line) and without dislocation walls (dotted red line) at room temperature, with voltage ranging from −200 V to 200 V. Inset: scheme of the contacts.

carried out at room temperature using a Keithley 6517 electrometer, with 0.2 V voltage step and 2 s settling time. The measurements were performed by ten-points averaging for each value. The crystals were both expected to show semi-insulating behavior. The crystal without dislocation walls has a higher resistivity, 1.5×10^9 Ωcm, in respect to 2.5×10^8 Ω cm in the samples with dislocation walls, with a lower leakage current of 100 nA compared to the current of 10 μA from the crystal with dislocation walls, when biased to ±200 V. These measurements are coherent with previous results which have shown that the dark current is higher on dislocation walls [9] in comparable samples.

2.2. PICTS measurements

It is worth noting that in this study we performed two different types of PICTS measurements. The first type is independent of the sign of the voltage applied and involves the use of a light pulse with wavelength corresponding to a photon energy below the bandgap of the samples. This first type [13] allows determining the concentration of the energy levels detected. The second type [14] strongly depends on the sign of the voltage applied and involves the use of a light pulse with photon energy above the bandgap of the samples. It allows distinguishing electron and hole traps.

2.2.1. PICTS measurements (first series)

It is worth reminding that the operating principle of the PICTS regards the analysis of the current transients when a light pulse is applied and the temperature increases at a constant rate, moving the Fermi level to the middle of the bandgap [13]. We will assume that, for a given temperature *T*, the light pulse ends at $t=0$. For $t>0$, the current I returns to the value before the light pulse with a transient. The current during this transient is measured at two different times $t_2 > t_1 > 0$ as a function of the temperature *T*. The normalized PICTS signal is defined as follows:

$$\text{PICTS } signal = \frac{I(T,t_2) - I(T,t_2)}{I(T,0)} = \frac{\Delta I}{IL_0} \quad (1)$$

where IL_0 is the current at $t=0$. When the PICTS spectrum has an extremum, a trapping level for the charge carriers is revealed, with the emission rate $e_{p,n}$ given by the following formula:

$$e_{p,n} = B \bullet \sigma_{p,n} \bullet T^2 \bullet \exp\left(-\frac{E_{act}}{K_B T}\right) \quad (2)$$

where *B* is a constant, K_B is the Boltzmann constant, $\sigma_{p,n}$ is the apparent capture cross section and E_{act} is the apparent activation energy.

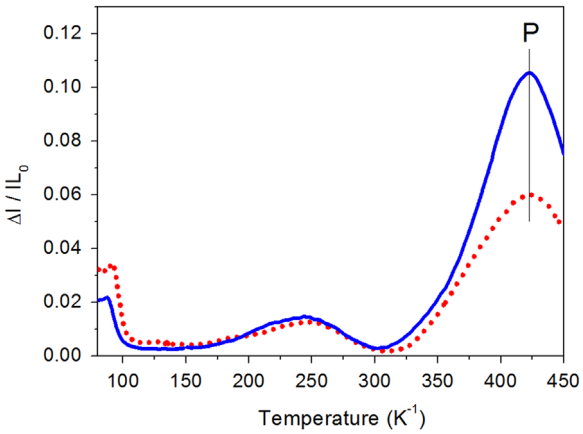

Fig. 3. Typical normalized PICTS spectra for the samples with dislocation walls (solid blue line) and without dislocation walls (dotted red line) obtained with applied bias 20 V, light pulses of 20ms, with photon wavelength 890 nm and emission rate 116.3 s^{-1}. The major maximum observed at high temperature is labeled *P*.

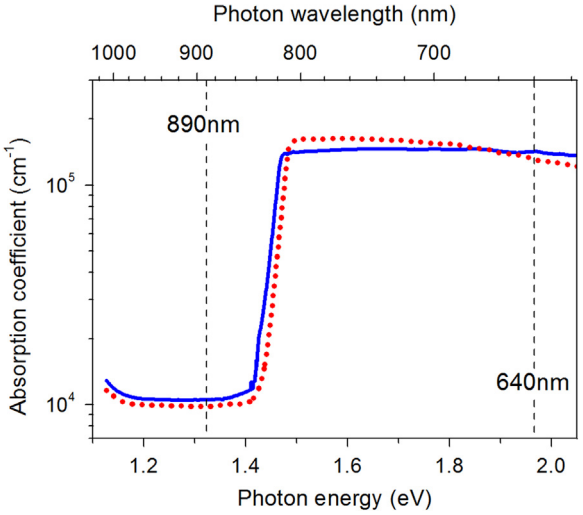

Fig. 4. Absorption coefficient α for the samples with dislocation walls (solid blue line) and without dislocation walls (dotted red line).

The PICTS measurements of the first type were performed on the crystals using a capacimeter-correlator from Sula Technologies, with 20ms light-pulses at 890 nm (corresponding to a photon energy of 1.39 eV, i.e. below the bandgap of the samples). For these PICTS measurements, two contacts in sandwich configuration were provided. The bottom-contact was ohmic, whereas the top contact was a semi-transparent Schottky Au contact.

Since the crystals under study are semi-insulating, during the measurements a constant applied bias equal to 20 V was applied, in order to obtain a detectable current signal ΔI.

Typical PICTS spectra obtained on the two types of crystals are shown in Fig. 3.

At low temperature, in the range 80–100 K, a maximum is observed. This is likely the energy level associated to the V_{Cd}^{2-}–Cl_{Te}^{+} complex, which is related to the compensation responsible for the high resistivity in CdTe [15,16,14]. Another broad maximum was observed in the range 160–270 K, that reasonably is the convolution of different peaks corresponding to different electronic energy levels [13]. The major maximum, labeled *P* in Fig. 3, is observed in the range 320–430 K, with much higher intensity than that of the other peaks. Since the concentration of defects, *N*, is responsible for a peak is directly proportional to the height of the peak observed in the normalized PICTS spectra, the maximum P should be generated by a defect whose concentration is higher in the samples with dislocation walls, compared to that of the samples without dislocation walls.

2.2.2. Concentration of PICTS levels

In order to establish the concentration *N* of the defects responsible for the observed level *P*, the following formula [17] was applied:

$$\frac{\Delta I}{IL_0} = \frac{N}{\Phi_0 \alpha}\left[\exp(-e_{p,n}t_1) - \exp(-e_{p,n}t_2)\right] \quad (3)$$

where Φ_0 is the incident photon flux and α is the absorption coefficient. Since *N* is severely dependent on the absorption coefficient, we performed measurements of absorption on the two kinds of samples to determine the value of α (Fig. 4) peculiar of our samples, using an alogen QTI lamp, a Cornerstone Monochromator 260 ¼m and a UTD PIN-10DFT silicon detector at room temperature.

The value of α corresponding to incident light with wavelength equal to 890 nm is 10615 cm^{-1} for the samples with dislocation walls and 9815 cm^{-1} for the samples without dislocation walls. These values are very close, that means the optical absorption properties of the two types of crystals are not significantly affected by the presence of dislocation walls.

The concentration of the defects responsible for the level *P* resulted 3.6×10^{14} cm^{-3} for the samples with dislocation walls and 1.5×10^{14} cm^{-3} for the samples without dislocation walls.

The concentration of the defect responsible for the level observed at 110 K was 7.2×10^{13} cm^{-3} for the samples with dislocation walls and 1.1×10^{14} cm^{-3} for the samples without dislocation walls. Since the low-temperature level might be the energy level associated to the V_{Cd}^{2-}–Cl_{Te}^{+} complex, it appears that the samples without dislocation walls are characterized by a greater Cl-compensation, which would contribute to the better semi-insulating behavior as measured by the resistivity values. This feature deserves future investigations to establish whether this energy level is actually associated to the V_{Cd}^{2-}–Cl_{Te}^{+} complex or to a defect of different nature..

2.2.3. PICTS measurements (second series)

Because of its broadness we investigated the possibility that the maximum *P* (Fig. 5(a) and (c)) is the convolution of two or more separate peaks. Therefore, we performed further PICTS measurements to go deeper into this subject. This second series of spectra was obtained with 20ms light-pulses at $\lambda = 640$ nm (1.93 eV, energy larger than the bandgap of the samples) in the high-absorption region. The bias applied to the face of the crystal subjected to the incident light was equal to +20 V for a first set of measurements and equal to −20 V for a second set. This allowed us to distinguish between energy levels acting as traps for holes, traps for electrons, or recombination centers, making it significant to perform a reliable deconvolution. The complete description of this technique is in reference [14]. Typical PICTS spectra obtained on the two types of crystals and corresponding Arrhenius plots are shown in Fig. 5, where a comparison of the spectra obtained with the first type of PICTS measurement (black line) and the second type of PICTS measurement (red and green lines) is provided. Normalized PICTS spectra are reported for the samples with dislocation walls (a) and without dislocation walls (c). The corresponding Arrhenius plots of the energy levels are shown in Fig. 5(b) and (d).

It is worth noting that the spectrum with an applied bias of −20 V on the samples without dislocation walls stops at 370 K because the signal to noise ratio was too low at higher temperature. By this method, three single peaks were observed, labeled *P*1, *P*2 and *P*3, the parameters of which are reported in Table 1.

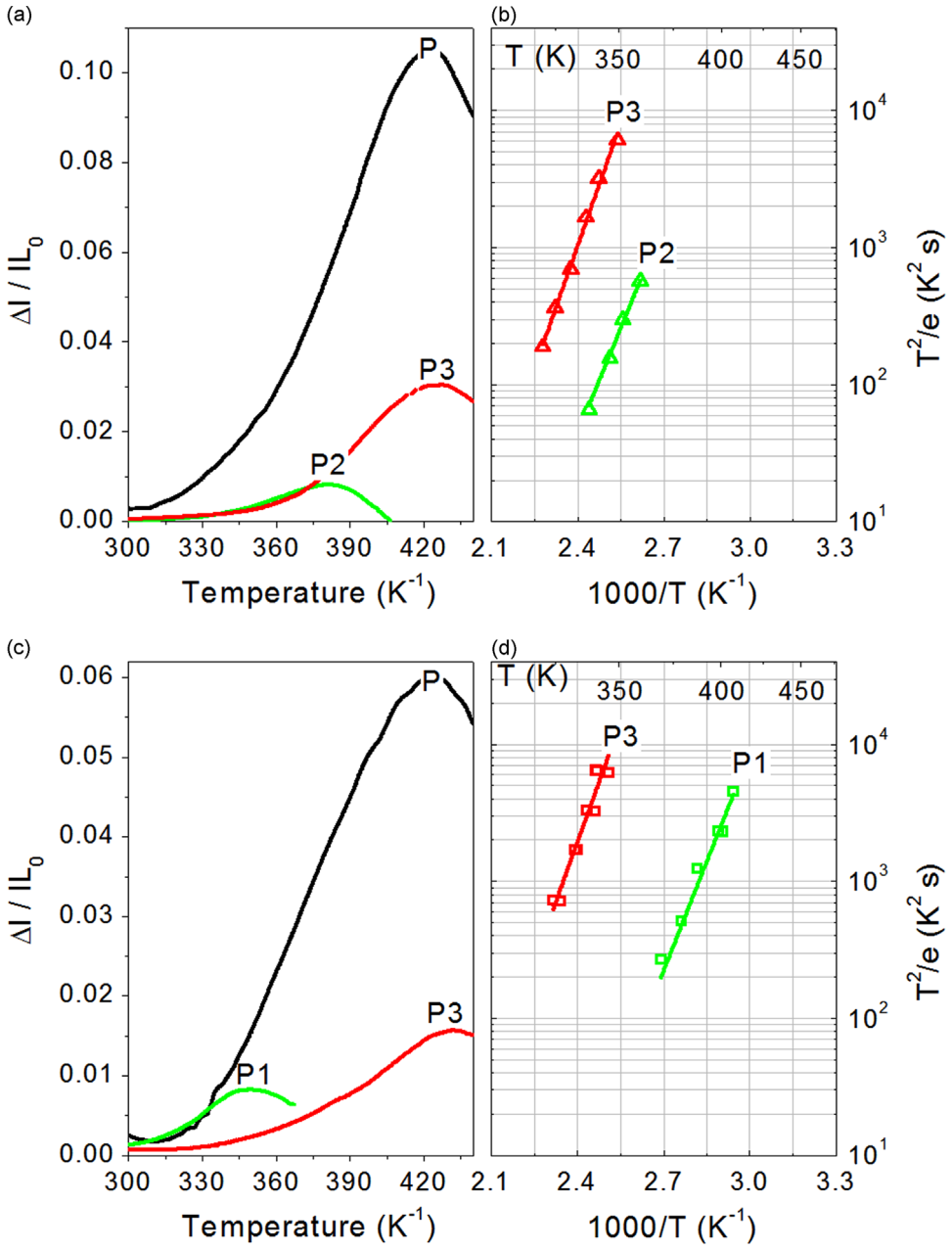

Fig. 5. Normalized PICTS spectra of the samples with dislocation walls (a) and without dislocation walls (c) with: (black line) applied bias 20 V, 20ms light pulses at wavelength 890 nm, emission rate 116.3 s^{-1}; (red line) applied bias +20 V, 20ms light pulses at wavelength 640 nm, emission rate 116.3 s^{-1}; (green line) applied bias −20 V, 20 ms light pulses at wavelength 640 nm, emission rate 116.3 s^{-1}. Arrhenius plots of the energy levels revealed for the samples with dislocation walls (b) and without dislocation walls (d).

Table 1
Parameters of the energy levels *P*1, *P*2 and *P*3.

Label	Activation energy (eV)	Capture cross section (cm^2)	Samples with dislocation walls	Samples without dislocation walls
P1	1.05	2×10^{-9}		Trap for electrons
P2	1.01	9×10^{-11}	Trap for electrons	
P3	1.15–1.18	$1–4 \times 10^{-10}$	Trap for holes	Trap for holes

2.3. Discussion

The level *P*3 was observed in both the crystals, with very close values of activation energy and apparent capture cross section. This level was observed only in the measurements with applied bias +20 V, and it is consequently attributable to a trap for holes. The levels *P*1 and *P*2 were observed in only one crystal at time: without dislocation walls and with dislocation walls, respectively. These two levels were observed only in the measurements with applied bias −20 V and they are, therefore, traps for electrons.

The trap levels have activation energies $E_{P1}=1.05$ eV, $E_{P2}=1.01$ eV, $E_{P3}=1.15–1.18$ eV and apparent capture cross sections $\sigma_{P1}=2 \times 10^{-9}$ cm^2, $\sigma_{P2}=9 \times 10^{-11}$ cm^2, $\sigma_{P3}=1–4 \times 10^{-10}$ cm^2.

The parameters for the energy levels observed are listed in Table 1. It should be noted that, although *P*1 and *P*2 have very close parameters, they are doubtless distinct energy levels since their peaks appear at different temperatures with the same emission rate.

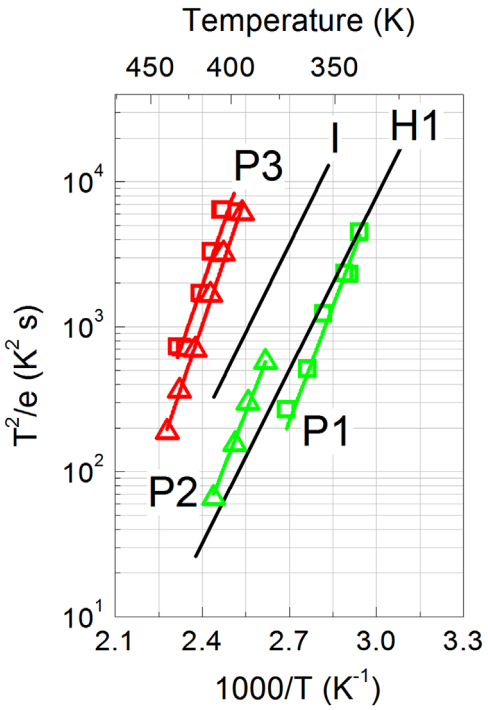

Fig. 6. Arrhenius plots of the energy levels revealed for the samples with dislocation walls (triangles) and without dislocation walls (squares) compared to the energy levels *H*1 and *I* in reference [16].

We hypothesize the origin of the observed energy levels to specific defects by comparing our results to the energy levels reported in literature:

1) The presence of one or more levels with activation energy around 1.0–1.1 eV in CdTe crystals was frequently reported in the past. Castaldini et al. [16] reported the presence of a level labeled I in CdTe, described as an electron trap with activation energy of 1.1 eV and attributed to V_{Te}^{+}, and a level labeled *H*1, described as a deep donor with activation energy E_C – 0.79 eV, detected only in chlorine doped CdTe and therefore attributed to Cl compensation.
   Although the Arrhenius plot fingerprints of these two levels are in the same region of the graph as the levels observed in this work (Fig. 6), there is not a precise correspondence. For what concerns the level *I*, no matching is found to the level *P*3; in addition to this, *P*3 is a trap for holes, whereas the level *I* was reported to be a trap for electrons. We can, therefore, exclude the correspondence of *P*3–*I*.
   On the other hand, the levels *P*1 and *P*2 almost superpose on the level *H*1, but their activation energy significantly differ. Since *H*1 was mainly observed by traditional DLTS measurements, we can hyphotise that *H*1 corresponds to the two splitted levels *P*1 and *P*2 detected by PICTS.
2) A broad photoluminescence emission at 1.1 eV was repeatedly reported in CdTe and CdZnTe [18–20]. Krustok et al. [20] investigated this emission peak in CdTe:Cl policrystalline samples and found it was constituted by two separated bands. These bands were attributed to donor–acceptor pairs, where the donor defect is at a Te site and the acceptor defect is at an interstitial position, possibly the V_{Te}–Te_i complex.
   The first band at 1.08 eV was reported to be present when the defect is surrounded by octahedral symmetry, while the second band at 1.17 eV was reported to be present when the pair is surrounded by tetrahedral symmetry. It must be pointed out that there is no agreement yet about this attribution, as widely described by Babentsov et al. [21].
   Nevertheless, on the basis of the matching of the activation energy, the level P3 observed in this work could be attributed to the first band found by Krustok et al., that is the V_{Te}–Te_i complex with tetrahedral symmetry.
   The levels *P*1 and *P*2 have activation energies very close to that of the second peak observed by Krustok et al. This would lead to the attribution of *P*1 and *P*2 to the V_{Te}–Te_i complex with octahedral symmetry, consequently assuming that the configuration of this defect is affected by the lattice rearrangement due to the dislocation walls. It is worth noting that differences in the energetic configuration of defects due to the presence of dislocation walls was already reported in the past, as for example in Ref. [22].

3. Conclusions

We performed current–voltage measurements, absorption measurements and PICTS analyses on chlorine doped CdTe crystals with two different densities of dislocation walls. The electrical measurements demonstrated that the absence of dislocation walls leads to better semi-insulating properties, since the samples without dislocation walls show lower currents at high voltages.

To the contrary, the optical absorption properties are very similar in the two samples which demonstrates that the dislocation walls unaffect the light absorption in the range of photon energy explored.

For what concerns the PICTS experiments, the low-temperature peak, likely the energy level associated to the V_{Cd}^{2-}–Cl_{Te}^{+} complex (which is related to the compensation responsible for the high resistivity of CdTe), has a higher concentration in the samples without dislocation walls. We hypothesize that this is due to an interaction between chlorine and dislocation walls (maybe gettering) which reduces the amount of chlorine available to form A-centers. However, this feature deserves a future specific investigation by extending the temperature range to lower limits. Furthermore, the high-temperature peak *P* was found to be a convolution of three single peaks, labeled *P*1, *P*2 and *P*3. Hyphoteses are advanced about the attribution of these three peaks.

Stating that, in the Arrhenius plot, the levels *P*1 and *P*2 superpose on the energy level labeled *H*1 found by traditional PICTS and DLTS measurements [18], we can hypotesise that the second type of PICTS measurements performed in this study resolved *H*1 so that it now appears as the convolution of two splitted levels.

For what concerns the nature of these levels *P*1 and *P*2, a possible correspondence was found, involving a donor–acceptor pair where the donor defect is at a Te site and the acceptor defect is at an interstitial position, possibly the V_{Te}–Te_i complex. In this view, *P*1 and *P*2 could be attributed to the V_{Te}–Te_i complex with octahedral symmetry, by assuming that the configuration of this defect is affected by the lattice rearrangement due to the presence of dislocation walls, whereas the level *P*3 could be attributed to the V_{Te}–Te_i complex with tetrahedral symmetry. Obviously, the proposed attributions are not conclusive, and we do not claim to have been exhaustive. However, it appears that the high-temperature region of the Arrhenius plot relevant to CdTe shows more levels than expected.

References

[1] L.R.S. Ladd, Infrared Physics 6 (1966) 145, http://dx.doi.org/10.1016/0020-0891(66)90008-X.
[2] L. Zou, Z. Gu, N. Zhang, Y. Zhang, Z. Fang, W. Zhu, et al., Journal of Material Chemistry 18 (2008) 2807, http://dx.doi.org/10.1039/b801418c.
[3] X. Wu, Solar Energy 77 (2004) 803, http://dx.doi.org/10.1016/j.solener.2004.06.006.

[4] K.L. Chopra, P.D. Paulson, V. Dutta, Progress in Photovoltaics: Research and Applications 12 (2004) 69, http://dx.doi.org/10.1002/pip.541.
[5] T. Schlesinger, J. Toney, H. Yoon, E. Lee, B. Brunett, L. Franks, et al., Materials Science and Engineering R: Reports 32 (2001) 103, http://dx.doi.org/10.1016/S0927-796X(01)00027-4.
[6] T. Takahashi, S. Watanabe, IEEE Transactions on Nuclear Science 48 (2001) 950, http://dx.doi.org/10.1109/23.958705.
[7] A. Castaldini, A. Cavallini, B. Fraboni, P. Fernandez, J. Piqueras, Physical Review B 56 (1997) 14897, http://dx.doi.org/10.1103/PhysRevB.56.14897.
[8] P.J. Sellin, A.W. Davies, a Lohstroh, M.E. Özsan, J. Parkin, IEEE Transactions on Nuclear Science 52 (2005) 3074, http://dx.doi.org/10.1109/TNS.2005.855641.
[9] C. Buis, G. Marrakchi, T.A. Lafford, A. Brambilla, L. Verger, E. Gros d'Aillon, IEEE Transactions on Nuclear Science 60 (2013) 199, http://dx.doi.org/10.1109/TNS.2012.2232306.
[10] C. Buis, E. Gros D'Aillon, a Lohstroh, G. Marrakchi, C. Jeynes, L. Verger, Nuclear Instruments and Methods in Physics Research Section A: Accelerators, Spectrometers, Detectors and Associated Equipment 735 (2014) 188, http://dx.doi.org/10.1016/j.nima.2013.08.084.
[11] C. Li, Y. Wu, T.J. Pennycook, A.R. Lupini, D.N. Leonard, W. Yin, et al., Physical Review Letters 111 (2013) 1, http://dx.doi.org/10.1103/PhysRevLett.111.096403.
[12] P. Rudolph, Crystal Research and Technology 40 (2005) 7, http://dx.doi.org/10.1002/crat.200410302.
[13] M. Tapiero, N. Benjelloun, J.P. Zielinger, S. El Hamd, C. Noguet, Journal of Applied Physics 64 (1988) 4006, http://dx.doi.org/10.1063/1.341361.
[14] X. Mathew, Solar Energy Materials and Solar Cells 76 (2003) 225, http://dx.doi.org/10.1016/S0927-0248(02)00276-3.
[15] V.S. Bagaev, Y.V. Klevkov, S.A. Kolosov, V.S. Krivobok, A.A. Shepel, Physics of Solid State 53 (2011) 1554, http://dx.doi.org/10.1134/S1063783411080051.
[16] A. Castaldini, A. Cavallini, B. Fraboni, P. Fernandez, J. Piqueras, Journal of Applied Physics 83 (1998) 2121, http://dx.doi.org/10.1063/1.366946.
[17] M. Ayoub, M. Hage-Ali, J.M. Koebel, R. Regal, C. Rit, F. Klotz, et al., Materials Science and Engineering: B: Advanced Functional Solid-State Materials 83 (2001) 173, http://dx.doi.org/10.1016/S0921-5107(01)00513-X.
[18] C. Davis, D. Allred, A. Reyes-Mena, J. González-Hernández, O. González, B. Hess, et al., Physical Review B 47 (1993) 13363, http://dx.doi.org/10.1103/PhysRevB.47.13363.
[19] W. Stadler, D. Hofmann, H. Alt, T. Muschik, B. Meyer, E. Weigel, et al., Physical Review B 51 (1995) 10619, http://dx.doi.org/10.1103/PhysRevB.51.10619.
[20] J. Krustok, V. Valdna, K. Hjelt, H. Collan, Journal of Applied Physics 80 (1996) 1756, http://dx.doi.org/10.1063/1.362981.
[21] V. Babentsov, J. Franc, E. Dieguez, M.V. Sochinskyi, R.B. James, IEEE Transactions on Nuclear Science 59 (2012) 1531, http://dx.doi.org/10.1109/TNS.2012.2191159.
[22] Y. Yan, M.M. Al-Jassim, T. Demuth, Journal of Applied Physics 90 (2001) 3952, http://dx.doi.org/10.1063/1.1405138.